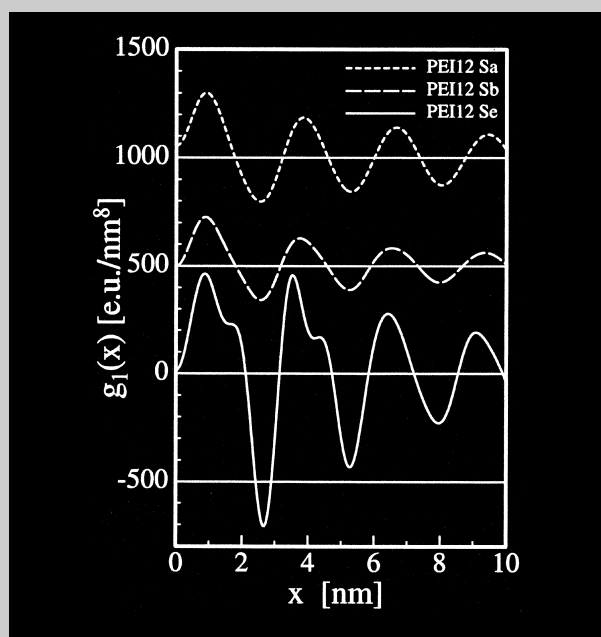


Full Paper: A poly(ester imide) (PEI) in the smectic crystalline (S_E) state exhibits both a medium-angle X-ray scattering (MAXS) peak and discrete small-angle X-ray scattering (SAXS). Based on quantitative analysis of absolute scattering data the observed SAXS is attributed to the formation of a sandwich structure in which a central, well-ordered layer-shaped zone is enclosed in disordered buffer zones. Additionally the MAXS of material in the frozen liquid-crystalline S_A and S_B states is analysed. The results show that the S_A state is characterised by long ranging correlation in the direction of the chain, whereas the lateral correlation range is short. Thus the smectic layer is considerably warped. The lateral range of order is wider in the S_B state and approaches infinity in the S_E state. This increase of lateral order and layer flatness goes along with considerable loss of longitudinal order. Nevertheless the range of longitudinal order remains high enough to assure correlation among the mesogens from the ordered zone with those from the disordered zones. Thus chain-folding cannot be the primary reason for the formation of ordered and disordered zones. Results indicate that asymmetry, orientation and internal twist of mesogenic groups in a liquid-crystalline main-chain polymer are important parameters controlling structure formation of the smectic morphology.



Interface distributions of the MAXS representing order and statistics of the smectic layer system.

Layer Morphology of a Poly(ester imide) LCP in Different Solid States

Norbert Striebeck,* Christoph Wutz

Institut für Technische und Makromolekulare Chemie, Universität Hamburg, Bundesstr. 45, 20146 Hamburg, Germany
Fax: +49-40-42838-6008; E-mail: Norbert.Striebeck@desy.de

Keywords: liquid crystalline polymers (LCPs); morphology; poly(ester imide); SAXS; smectic

Introduction

Since liquid crystallinity in polymers (liquid crystalline polymers, “LCPs”) was first recognised, enormous effort has been made to investigate different phase morphologies and the transitions among them. In this process conflicting phenomena were observed, which ask for a refinement of structural notions. One of these conflicts arises from the finding that LCPs may show a clear small-angle X-ray scattering (SAXS) reflection related to a long period which is several times greater than the unit repeat computed by summing the lengths of mesogen and spacer.

Antonietti et al.^[1] have studied films of poly(*N*-alkyl acrylamide)s with various spacer lengths. For all their

samples they observed a discrete small-angle scattering, which varies strongly as the spacer length increases. The authors attribute this variation to both an increasing phase separation and a considerable change of morphology. Consequently, they focus on the topology of the phase-separated system and develop a novel data-evaluation method which allows the assessment of global topological features from a SAXS powder pattern.

Early investigations of main-chain LCPs with an alternating sequence of regular mesogen and spacer units have shown that the structural feature most frequently observed is the expected layer topology. In 1985 Thomas and Wood^[2] investigate the solid-state morphology of poly(hexamethylene *p,p'*-bi-benzoate) (BB-6). They find

a smectic topology built from alternating mesogen and spacer layers. In crystallised samples they, additionally, observe a superstructure and attribute it to a structure built from alternating super-layers of perfect and imperfect structure, respectively. In 1989 BB-6 was investigated by Takahashi and Nagata,^[3] who for the first time report the observation of a SAXS peak which corresponds to the mentioned superstructure. In two further papers^[4,5] the increase of the long period as a function of annealing temperature is studied and attributed to chain-folding at the surface of the super-layers.

In 1992 Murthy and Aharoni^[6] studied poly(ester amide)s and observed “diffuse and weak SAXS reflections with spacings longer than the chain-axis repeat”. They attribute the peaks to a lamellar structure in which ordered layers of hydrogen-bonded sheets are separated by less ordered domains. By combined annealing and swelling in a solvent they can establish various long periods. All of them are multiples of the basic unit repeat of the LCP. In the same year, a similar multiplicity of possible long periods is reported by Mensinger et al.^[7] from grafted LCPs. Most of the cited papers discuss the question: if the formation of “super-lamellae” during crystallisation of LCPs can be explained by regular chain folding, or if the chains appear to cross ordered and disordered zones in a more or less extended fashion. Chain-folding is unanimously favoured. Quantitative analysis of both SAXS and MAXS employing the concept of interface distribution functions^[8,9] lead us to the opposite conclusion. Chain folding cannot be located at the surface of the well-ordered super-lamellae.

Experimental Part

Materials

The studied poly(ester imide) material (“PEI12”) was synthesised in the group of Kricheldorf.^[10,11] A model of the repeat unit is shown in Figure 1.

It comprises the mesogen (to the left) and the spacer with 12 CH₂ groups (to the right). The single chain conformation was modelled using a consistent-valence force field (for additional conformations obtained with other forcefields (cf. ref.^[12] p. 86). The mesogen is asymmetric and twisted. The extended spacer (1.65 nm) is longer than the mesogen (1.34 nm). The unit repeat is 2.94 nm.

Samples were prepared by melting the polymer in a heat press at 200 °C under a vacuum for 2 min and pressing the melt into a film of approx. 200 µm thickness, which was immediately quenched in ice water. This treatment yields material in S_A state (smectic A), a frozen liquid-crystalline phase (sample designation “Sa”). Part of this material was annealed under two different conditions, resulting in two additional samples: annealing for 12 h at 90 °C yielded sample “Sb” in the S_B state; annealing for 12 h at 135 °C yielded sample “Se” in the frozen smectic-crystalline state S_E.

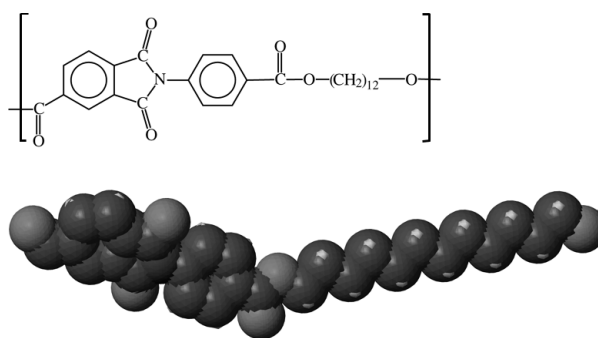


Figure 1. PEI12 material unit repeat.

A fourth sample, “Sem”, was prepared by slowly cooling the melt in the heat press. It has been verified^[12,13] that this procedure yields material in the S_E state, as well.

Method

SAXS was performed in a Kratky compact camera (Anton Paar AG, Graz, Austria) employing Ni-filtered CuK_α radiation and a proportional counter. An entrance slit-height of 80 µm was chosen and an angular range $1.3 \cdot 10^{-2} \text{ nm}^{-1} \leq s \leq 1.1 \text{ nm}^{-1}$ was scanned. Here $s = (2/\lambda) \sin \theta$ and is the modulus of the scattering vector. In the plane of registration the length of the slit was 2.01 nm^{-1} measured in units of the scattering vector. Calibration of the intensity to absolute units was carried out using the moving-slit device, as described in earlier work.^[14] In order to improve the signal-to-noise ratio of the data several pieces of film were stacked and mounted in the sample holder.

Results and Discussion

Observed Scattering

Figure 2 shows slit-smearred raw data recorded from a Kratky camera after background elimination in absolute intensity units.

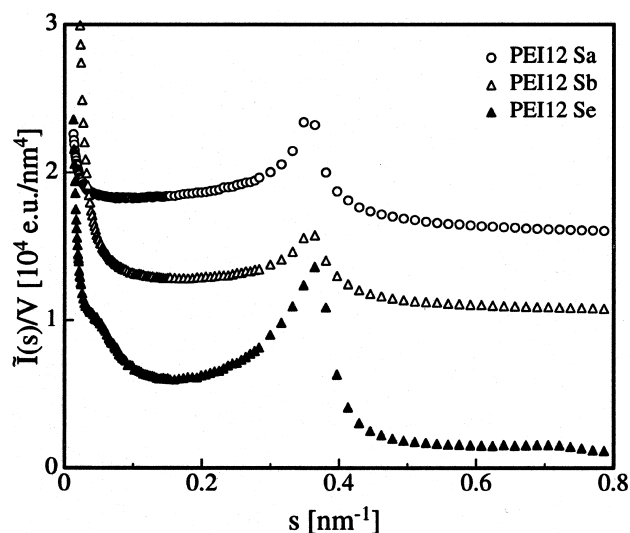


Figure 2. Slit-smearred scattering intensity $\bar{I}(s)/V$ in absolute units. Curves are stacked for clarity.

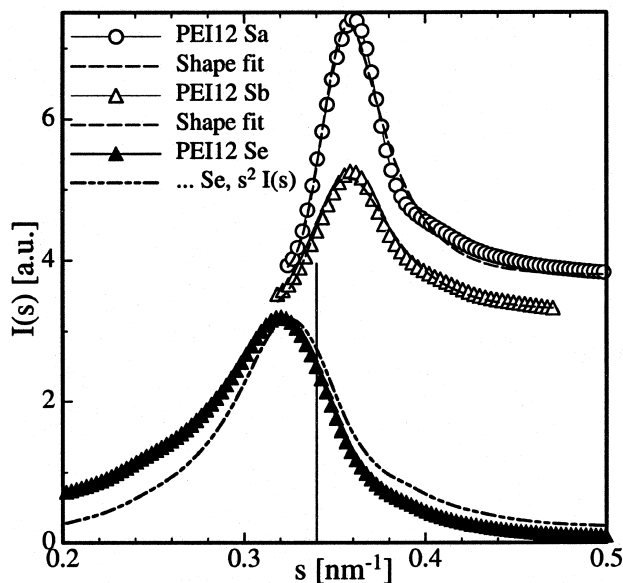


Figure 3. Point-collimation data: The main peak of the MAXS after deconvolution (symbols). For samples *Sa* and *Se* dashed lines show fits of the line shape. For the bottom curve of sample *Se* the dashed line represents the “Lorentz-corrected” intensity, $s^2 I(s)$. The vertical line indicates the position of the unit repeat in reciprocal space.

Sample *Sa* shows the scattering of the smectic layer system with a pronounced maximum at $s \approx 0.38 \text{ nm}^{-1}$. The scattering of sample *Sb* is similar, but additionally diffuse SAXS is observed in the vicinity of zero scattering angle. Sample *Se* exhibits discrete SAXS with a long period reflection at $s \approx 0.05 \text{ nm}^{-1}$.

The curves from sample *Sem* (smectic E crystallised from the melt) and *Se* (smectic E crystallised from the frozen LC state) look similar.

MAXS Peak Shape Analysis

In Figure 3 the main peaks of the MAXS after numerical slit length desmearing are shown. All curves are asymmetric.

Similar asymmetry has been observed with a point-focus collimation, when the melting behaviour of the material was studied.^[12, 13]

As has been pointed out earlier,^[15] the main reason for this asymmetry is anisotropy of order in the lattice of smectic layers. This fact was deduced from comparing scattering patterns of drawn fibres with scattering curves of isotropic material. Only in the smectic E state (sample *Se*) the mesogen layers are flat. In this case “Lorentz correction” of the isotropic curve compensates the effect of the spherical average of a point reflection. Result is a symmetrical peak. To a first approximation, the inverse of the integral width of this peak is h_s , the height of the correlated stack of layers (“Scherrer equation”).

In the smectic A and B states the layers are warped in some regular or irregular fashion, and the corresponding

Table 1. MAXS peak–shape analysis. Model fitting was performed for samples *Sa* and *Sb*. For samples *Se* and *Sem* the width of the Lorentz-corrected peak was analysed. P is proportional to the peak integral. R is the unit repeat (MAXS long period). h_s is the height of the smectic layer stack. r_f is the radial range of flatness of the (mesogen) layer.

Samples	P	$\frac{R}{\text{nm}}$	$\frac{h_s}{\text{nm}}$	$\frac{r_f}{\text{nm}}$
<i>Sa</i>	5.2 ± 0.2	2.9 ± 0.2	27 ± 2	1.6 ± 0.4
<i>Sb</i>	2.2 ± 0.1	2.9 ± 0.2	20 ± 1	1.6 ± 0.4
<i>Se</i>		3.1 ± 0.2	9	∞
<i>Sem</i>		3.1 ± 0.2	11	∞

MAXS of oriented material resembles a layer line. Here the effect of the spherical average is not easily compensated. In a related paper^[15] we present an analytical solution for the peak shape, which is a function of two parameters, r_f , the radial range of flatness, and h_s . These parameters describe radius and height of a cylinder, respectively, forming the anisotropic correlation body of the layer lattice. Two extra parameters in the model describe the integral peak intensity, P , and the unit repeat, R , which defines the peak position.

It should be mentioned that r_f could as well be interpreted in terms of a sharp boundary of the smectic layer in lateral direction. Following this interpretation the notion of layers would have to be abandoned for the non-crystalline samples. This would lead to a contradiction to evidence^[16] from other methods, because basic requirement for a smectic phase is the arrangement of mesogens forming layers. Only if we were to disregard this prerequisite and, moreover, we were to entertain the notion of almost planar layers, could we utilize the method of Burger^[1, 17] to determine a most-probable mesophase morphology from peak shape by an expansion of the correlation function.

Fits by the model function are shown for the upper two curves in Figure 3. The resulting parameter values are presented in Table 1.

Because there are various effects causing peak-broadening, the presented values are lower limits. One observes that for the non-crystalline smectic phases *Sa* and *Sb*, the unit repeat R is in excellent agreement with the value computed by molecular modelling of a free chain without interactions. In Figure 3 the corresponding position is indicated by a vertical line. From the Figure it becomes obvious that picking R from the peak maximum or from its centre of gravity would result in systematic error. For the samples *Se* and *Sem*, the peak position appears to indicate a more stretched conformation of the repeat unit. This modelling does not consider statistical variation of layer thicknesses and repeat units which is very important in common polymeric multiphase systems. For the smectic layer stack we assume this effect to be of minor importance. Nevertheless, we will analyse and discuss the influ-

ence of layer statistics in the sequel. Because a layer system is at least a two-phase system, we start with an extraction of the multiphase feature from the scattering data.

Multiphase Systems

All samples show a pronounced Porod law in the MAXS range. The upper limit of the interval is not accessible in the Kratky camera. The samples *Se* and *Sem* show a second Porod law in the SAXS range. This Porod region ends at $s_{\max} = 0.16 \text{ nm}^{-1}$. Thus it appears reasonable to interpret the data in terms of multiphase systems. Following the concept of Ruland^[9, 18, 19] the non-ideal character of the multiphase system is evaluated and described by the two parameters w_i (width of the transition zone between the phases) and I_{Fl} (density fluctuation background). In the same evaluation step \bar{A}_p is determined. \bar{A}_p governs the asymptotic decay of the slit-smear scattering intensity according to Porod's law. Table 2 shows the values determined. It shall be pointed out that the fluctuation background for the SAXS regime (two bottom rows) is remarkably high. This finding can be related to an "inner structure" of the phases seen by the SAXS, which shows up in the discrete MAXS. Using the determined parameter values the slit-smear interference function $\tilde{G}_1(s)$ of the ideal multiphase system is computed, as has been described in earlier work^[9] (cf. Figure 4).

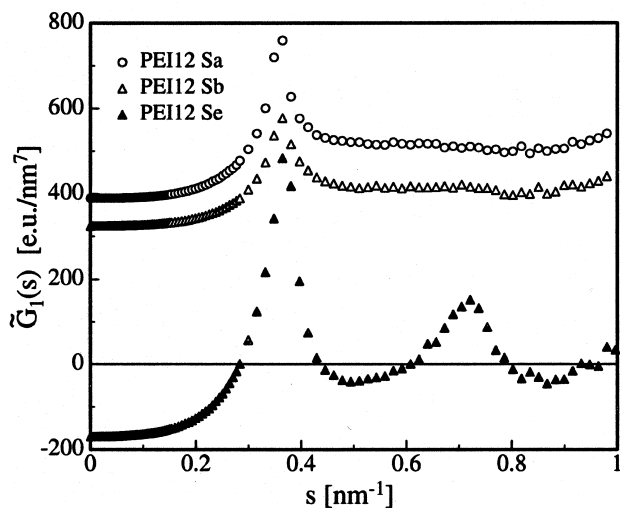


Figure 4. Interference functions $\tilde{G}_1(s)$ computed from the slit-smear scattering intensity are a representation of the ideal multiphase system. Curves are stacked for clarity.

Observable Features of MAXS Interface Distributions

Interface distribution functions $g_1(x)$ (IDF)^[8] are computed by Fourier-Bessel transformation from $\tilde{G}_1(s)$. The IDF is suitable for the analysis of lamellar systems. As we have learned from the study of fibres and MAXS peak shape, in the smectic A and smectic B state the layers are warped and thus we should be aware of possible systematic errors. Figure 5 shows the IDFs computed from the

Table 2. Parameters from the analysis of Porod's law. The top four rows display data from the analysis of the MAXS. The two bottom rows* refer to the analysis of the discrete SAXS, which is only present in the scattering of samples in the smectic E state. \bar{A}_p is the Porod asymptote governing Porod's law, w_i is the width of the transition zone between phases and I_{Fl} the fluctuation of the electron density within a phase.

Sample	\bar{A}_p e.u. · nm ⁻⁷	w_i nm	I_{Fl} e.u. · nm ⁻³
<i>Sa</i>	110 ± 20	0.4 ± 0.2	430 ± 10
<i>Sb</i>	75 ± 3	0.35 ± 0.05	330 ± 5
<i>Se</i>	170 ± 30	0.5 ± 0.3	435 ± 15
<i>Sem</i>	150 ± 30	0.1 ± 0.4	350 ± 40
<i>Se*</i>	0.64 ± 0.05	0.7 ± 0.4	2930 ± 20
<i>Sem*</i>	0.90 ± 0.05	0.7 ± 0.1	2235 ± 40

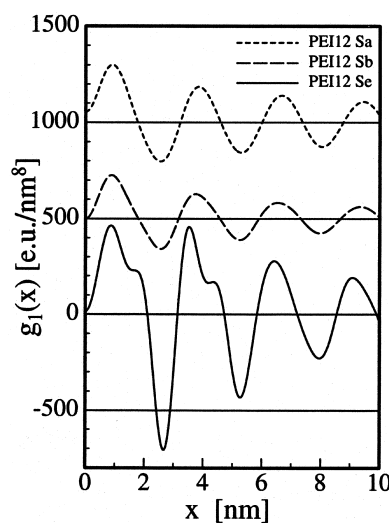


Figure 5. Interface distributions of the MAXS representing order and statistics of the smectic layer system.

MAXS of the samples. All curves show many regular oscillations, as is typical for a lattice with some range of order. The curves from samples *Sa* and *Sb* do not show many details. In the *Se* state (as well as in the *Sem* state) the curve starts with two positive peaks which can be associated to the thickness distributions of the mesogen layer and of the spacer layer, respectively. The first negative peak represents the distribution of the unit repeat. The next two positive peaks are clearly separated. A striking peculiarity is observed: The left positive peak in this block is significantly narrower than each of the peaks in the first block. Such finding can only be explained by a complex multiphase structure with interacting neighbouring layers. Nevertheless, the overall regularity shows that the general scheme of mesogen-spacer repeat is preserved.

Layer-Structure Analysis

In previous work^[9, 19–21] we demonstrated how the structure of a layer system can be described by means of one-

dimensional structural models based on layer-thickness distributions and on one-dimensional statistics. Such models can be fitted to the IDF. Lattice statistics define an average lattice constant \bar{R} first, and assume that individual unit repeats R fluctuate about this mean value. Second, a decorating layer is placed onto the lattice points, the thickness of which is subject to fluctuations, too. Stacking statistics assume that the basic entities of structure are the two thicknesses of mesogen and spacer layers, respectively, which both are subject to fluctuations. Lattice and stacking statistics were first discussed by Hermans.^[22] A third statistical model can readily be unified with both.^[9] First proposed by Kochendörfer and Dehlinger^[23] in crystallography it was named “homogeneous stress distribution”. When adopted into the field of SAXS it was given various names.^[24–26] Let us name the model “*homogeneous long period distribution model*” (*hL model*) following Ruland. Kochendörfer and Dehlinger exploited the idea that a mean structure may be distorted (compressed or expanded) from varying local stresses. Thus the locally different stresses cause the sample to appear inhomogeneous and the global lattice constants vary continuously in some range. The standard deviation σ_H of this global fluctuation characterises the heterogeneity of the sample.

MAXS-IDF Analysis of Non-Crystalline Samples

Applied to our non-crystalline samples we find that the lattice model is clearly better than stacking statistics and fits the IDFs of both samples perfectly. The results of the fits for the samples *Sa* and *Sb* are collected in Table 3.

We observe that the layer structure of both samples can be described by pure lattice statistics ($\sigma_H = 0$). For both samples the average lattice constant \bar{R} is about 2.65 nm and fluctuates by about 15% (σ_R/\bar{R}). This result is in excellent agreement with the result of peak shape analysis. Surprisingly the thickness \bar{t}_m of the mesogen layer is considerably lower than the length of the mesogen itself and fluctuates over a wide range. In order to explain this finding, a minimum of two assumptions is necessary: (1) A considerable part of the individual mesogens sticks out from the common layer. (2) The inevitable mixed phase

Table 3. Structural parameters determined from the fits of the IDFs of the non-crystalline samples *Sa* and *Sb*. \bar{R} average unit repeat (lattice constant). \bar{t}_m average thickness of the mesogen layer (decorating phase). σ_R/\bar{R} relative variance of the lattice constant. σ_m/\bar{t}_m relative variance of the mesogen layer thickness. σ_H skewing parameter for the thickness distributions.

Samples	$\frac{\bar{R}}{\text{nm}}$	$\frac{\bar{t}_m}{\text{nm}}$	σ_R/\bar{R}	σ_m/\bar{t}_m	σ_H
<i>Sa</i>	2.66 ± 0.04	0.83 ± 0.02	0.14 ± 0.01	0.72 ± 0.03	0
<i>Sb</i>	2.62 ± 0.03	0.84 ± 0.01	0.16 ± 0.01	0.57 ± 0.02	0

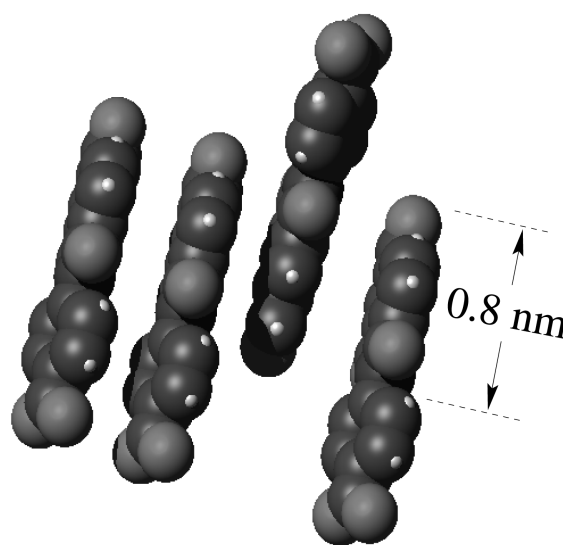


Figure 6. An arrangement of shifted mesogens of PEI12, which generates a layer with a thickness of 0.8 nm.

requires some extra volume. Since the mesogen shape is twisted and asymmetric with random orientation, this finding appears not to be unreasonable. A possible conformation of mesogens in the layer is sketched in Figure 6.

While a two-phase layer model appears to be suitable to fit the IDFs of the non-crystalline samples, fits of the semicrystalline samples *Se* and *Sem* based on this simple model are not satisfying. The IDFs of the semicrystalline samples exhibit so many details that it appears to be practical to define a more complex multiphase model and to fit this to the IDFs. One hint on how this model can be constructed is in the result of MAXS peak shape analysis: Particularly for the semicrystalline samples the correlation height of the lattice is low, and thus a finite model with a limited number of correlated layers should suffice. But even in this case we have to answer another question before we can start to build a model for the MAXS: how is the bunch of phases chained into a sequence along the stack of layers? Because this question is answered by analysis of the discrete SAXS, we defer MAXS modelling until the SAXS results are analysed.

SAXS-IDF Analysis of Semicrystalline Samples

One of the SAXS IDF curves and its best fit with a two-phase model is shown in Figure 7.

We remember that for the MAXS IDFs the lattice model fits perfectly. For the SAXS IDF of sample *Se* the stacking model is more favourable. But the stacking statistics are peculiar: one of the two super-layer thickness distributions is rather narrow and symmetric, while the other one is extremely asymmetric in the sense of the mentioned “stress broadening”. We identify the sym-

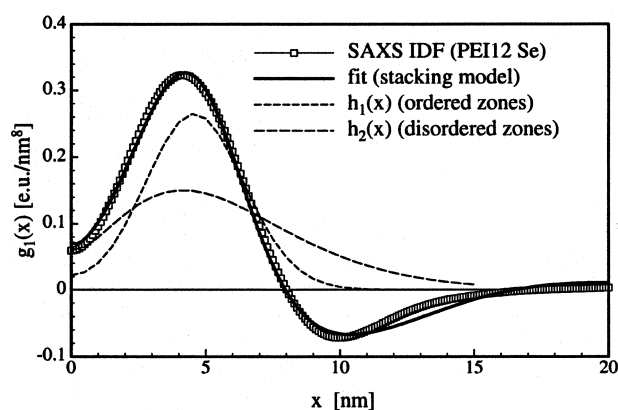


Figure 7. Best fit of the SAXS IDF of sample *Se*. Dashed curves show the thickness distributions $h_1(x)$ and $h_2(x)$ of both phases, decomposed from the fit parameters.

metric distribution as an ordered zone and the asymmetric distribution as a strongly disordered zone surrounding the ordered zones. We observe that there is no correlation beyond $x = 15$ nm, which is in excellent agreement with the result from MAXS peak-shape analysis. The severe asymmetry of the thickness distribution of the disordered zones means that there is a minimum range of disorder surrounding every ordered zone, but that there is no definite upper limit for its thickness. This fact suppresses correlation among the ordered zones. Thus the observed discrete SAXS of the semicrystalline samples is caused from a simple sandwich structure: Every ordered zone is encapsulated in disordered zones. The structural parameters of the fits are collected in Table 4.

Sample *Se* has been crystallised from the quenched *Sa* state, while sample *Sem* has been crystallised from the isotropic melt. The comparison yields similar average thicknesses of ordered and disordered zones, but the layer statistics are quite different. Sample *Sem* exhibits the pure case of a “homogeneous long period distribution model”, and this means that here we face a structure, in which the expanded and compressed images of an average lattice are present in the heterogeneous sample. The lattices are made from alternating ordered and disordered zones, with every disordered zone being $\bar{t}_d/\bar{t}_0 = 1.4$ times as wide as the related ordered zone. Here the predominant

structural feature is the close correlation between the width of an ordered zone and the widths of the surrounding disordered zones. For both samples the average width of the ordered zone is somewhat smaller than the double layer repeat \bar{R} , revealing that pairs of crystallised mesogen layers appear to be the most frequent typification of the ordered zones.

MAXS-IDF Analysis of Semicrystalline Samples

The information gathered in the previous section should suffice to build a multiphase model and test it with the MAXS data of the semicrystalline samples. Nevertheless, there is basic difference between the samples if stacking statistics is considered. While there is so much disorder in sample *Se* that a fair fit should be possible, if the model considers only ordered double layers, the *hL* model statistics of sample *Sem* requires, in principle, a superposition of lattices which differ by the cluster sizes for the ordered zones within an estimated range of one to four crystallised layers. Such model is very complex and the physical meaning of extracted parameters strongly depends on necessary assumptions concerning the superposition. Therefore we have only fitted the data of sample *Se* and built a model which is based on ordered zones comprising only two crystalline mesogen layers. Most probably the electron density of crystallised mesogen layers will differ from that of corresponding layers with liquid-crystalline disorder. Following this notion a three-phase model (spacer phase, disordered mesogen phase and crystalline phase) has been tested. But this model is not much better than the simple two-phase model. Only a five-phase model results in reasonable fits. It is sketched in Figure 8. We assume that the spacer layer between crystallised layers exhibits a different density than the spacer layer between two disordered mesogen layers. Consequently the spacer layer at the interface between ordered and disordered zone comes with a density of its own. The step heights are adapted by the regression algorithm and the sketched relative step heights and layer thicknesses correspond to the result of the fit.

By convention the relative contrast between liquid-crystalline layer and spacer layer is set to unity. Three other step heights are fit parameters. Absolute step heights are controlled by a general weighting factor W . The model function comprises 10 fit parameters. The fit of sample *Se* results in the following parameter set: $W = 62 \pm 8$ e.u. \cdot nm $^{-7}$ for the overall weight, $\bar{t}_1 = 0.38 \pm 0.04$ nm for the average thickness of the liquid-crystalline layer, $\bar{t}_c = 0.76 \pm 0.04$ nm for the thickness of the crystalline layer, $\bar{R} = 2.65 \pm 0.01$ nm, $\sigma_1/\bar{t}_1 = 0.54 \pm 0.01$ for the relative variation of the liquid-crystalline layer thicknesses, $\sigma_c/\bar{t}_c = 0.36 \pm 0.01$ for the relative variation of the thicknesses of crystalline mesogen layers, $\sigma_R/\bar{R} = 0.09 \pm 0.01$ for the relative fluctuation

Table 4. Structural parameters determined from the fits of the SAXS IDFs of the semicrystalline samples *Se* and *Sem*. \bar{t}_0 average thickness of the ordered zone. \bar{t}_d average thickness of the disordered zones. σ_0/\bar{t}_0 relative variance of the ordered zone. σ_d/\bar{t}_d relative variance of the disordered zones. σ_H skewing parameter for the thickness distributions.

Samples	\bar{t}_0 nm	\bar{t}_d nm	σ_0/\bar{t}_0	σ_d/\bar{t}_d	σ_H
<i>Se</i>	4.6 ± 0.1	5.6 ± 0.1	0.06 ± 0.06	0.44 ± 0.03	0.40 ± 0.02
<i>Sem</i>	4.2 ± 0.2	5.9 ± 0.3	0	0	0.44 ± 0.04

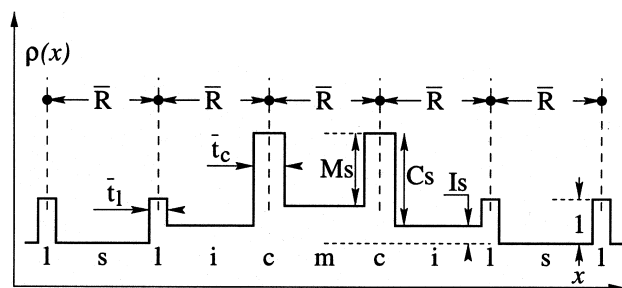


Figure 8. Average structure of the five-phase model, which allows the fit of the MAXS IDF of the semicrystalline PEI12 sample *Se*. Surrounding the ordered zone with two crystallised (c) mesogen layers of thickness \bar{t}_c there are always liquid crystalline (l) layers with an average thickness \bar{t}_l . Both kinds of layers decorate a paracrystalline lattice with the average unit repeat \bar{R} . Relative step heights are indicated by vertical arrows: Middle step (Ms), crystal step (Cs) and interfacial step (Is).

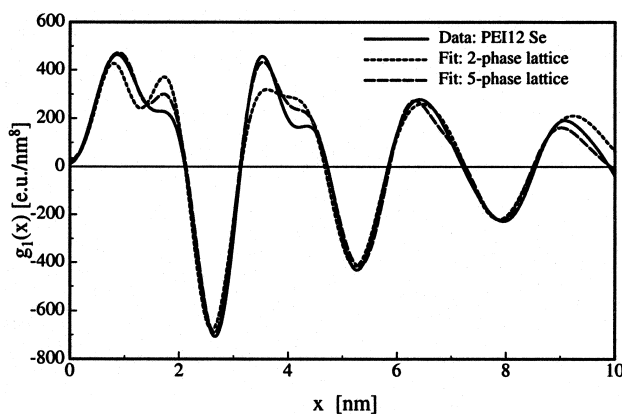


Figure 9. MAXS IDF of the semicrystalline sample PEI12 *Se* and its fits using two-phase and five-phase models of layer statistics, respectively.

of the unit repeat, $I_s = -0.37 \pm 0.05$ for the relative change of contrast in the interfacial step, $C_s = 1.85 \pm 0.22$ and $M_s = -0.76 \pm 0.14$ for the remaining steps. Fits are visualised in Figure 9.

The simple two-phase model does not fit the data. The five-phase model fits the IDF quite well, but there are systematic deviations between the fit and the measured data, which are concentrated in the vicinity of two peaks of the IDF. The first deviation occurs in the second positive peak, which is associated to $\bar{t}_s = \bar{R} - \bar{t}_c$, the average thickness of spacer layers. The second deviation is observed in the fourth positive peak, which is associated to a sub-stack of one mesogen layer surrounded by a spacer layer on each side. We observe that in both cases the model supplies less area for these peaks than is required to fit the measured data. Thus to improve the fit we would have to add some structure to the model defined so far. Because the addition only affects single crystalline layers and their surrounding spacer layers, the required additional structure is readily identified as a small fraction of volume in the sample filled by single

crystalline mesogen layers surrounded by disordered zones. We feel that a quantitative analysis of this faint component would put too great a strain on the recorded data.

Because the correlation height of the stack from alternating mesogen and spacer layers is much higher than the height of the ordered zone, chain folding cannot be the primary reason for the formation of ordered and disordered zones.

The Structure of Sample *Se*

Since the parameters found in the fit of sample *Se* describe the structure almost completely and the measurements have been performed in absolute units of the scattering intensity, electron density differences (contrasts) between all phases can be computed in absolute units. Volume fractions of the phases can be computed from the layer thicknesses, and relative contrasts can be determined from the step heights. Then the invariant Q can be used to calibrate the contrasts to absolute units. The computation of Q by integration of the isotropic scattering curve is well-known. We extrapolate the integrand towards zero scattering angle and use the Porod's asymptote, \bar{A}_p , for the purpose of extrapolation towards infinity, as has been proposed by Ruland.^[18] For an m -phase system the equation

$$Q = \sum_{i=1}^{m-1} \sum_{j=i+1}^m \phi_i \phi_j (\Delta\rho_{ij})^2$$

describes the relation between the volume fractions ϕ_i and the contrasts $\Delta\rho_{ij}$ between the i^{th} and the j^{th} of the m phases. The model fit results in values for $\Delta\rho_{ij}$ in relative units. Setting the relative model invariant equal to the absolute invariant of the scattering yields the calibration constant. Results are collected in Table 5 and enable to

Table 5. The phases of PEI12 in the states, *Sa*, *Sb* and *Se* as determined from MAXS IDF analysis. Phase denomination according to Figure 8. Electron densities ρ_{el} (By convention the density of a free spacer layer is set to zero) and volume fractions ϕ_k . Thicknesses \bar{t}_k and variances σ_k/\bar{t}_k of lattice decorating phases are presented.

Sample	phase	$\frac{\rho_{el}}{\text{e.u.} \cdot \text{nm}^{-3}}$	ϕ_k	$\frac{\bar{t}_k}{\text{nm}}$	σ_k/\bar{t}_k
<i>Sa</i>	spacer (s)	0	0.69		
	LC (l)	134 ± 4	0.31	0.83 ± 0.02	0.72 ± 0.03
<i>Sb</i>	spacer (s)	0	0.68		
	(l)	114 ± 1	0.32	0.84 ± 0.01	0.57 ± 0.02
<i>Se</i>	spacer (s)	0	0.33		
	LC (l)	98 ± 13	0.11	0.38 ± 0.04	0.54 ± 0.01
	interface (i)	62 ± 9	0.31		
	crystalline (c)	242 ± 39	0.11	0.76 ± 0.04	0.36 ± 0.01
	middle (m)	169 ± 34	0.14		

assess the global shifts among volume fractions on one hand and densities on the other hand, which are related to transitions among the investigated morphological states of PEI12.

The transition from *S_a* to *S_b* decreases the contrast between spacer phase(s) and mesogen layer (l). The now lighter packing in the hexagonal phase goes along with more uniform thicknesses of the mesogen layer and thus with a smaller inner surface. Thus phase separation is improved at the cost of a lighter packing of the twisted and bulky mesogens.

Passing into the semicrystalline smectic E state, 1/3 of the LC mesogen phase is crystallised, 1/3 remains in the phase-separated liquid-crystalline state, and 1/3 is dissolved in the spacer phase. Thus the crystallising lamella in its close environment enforces partial mixing of spacer segments with mesogenic groups. Even in the crystallised state the thickness of the mesogen layer is only a fraction of the total mesogen length, which appears to be the longest possible match length. Since this length is almost the same in all three states, crystallisation as a whole results in a considerable deterioration of phase separation between the incompatible segments of the chain. The conservation of the match length means that the decrease of specific volume in the crystallising layers solely propagates by lateral contraction and levelling out of the warped layer surfaces. Further evidence for such short match length is presented by Gieseler.^[27] From the analysis of WAXS fibre patterns from PEI12 she finds that the unit cells *c*-axis is only 0.8 nm high.

The general structural features of the samples *S_e* and *S_{em}* appear to be similar, the main difference being that in *S_e* almost all the ordered zones are built from pairs of smectic-crystalline layers, whereas in *S_{em}* we observe a broad distribution of widths with considerable amounts of ordered zones built from triplets and singulets of smectic-crystalline layers as well.

Conclusions

The study shows that quantitative analysis of the absolute SAXS and MAXS of unoriented LCPs can contribute to elucidation of the complex structure built from mesogen and spacer layers.

Compared to the results of other authors obtained on different polymers,^[4-7] this study indicates that asymmetry, orientation and internal twist of mesogenic groups in a LC main-chain polymer are important parameters controlling structure formation of smectic morphology.

Acknowledgement: We thank Professor H. R. Kricheldorf for kindly providing the investigated material.

Received: August 29, 2001

Accepted: September 11, 2001

- [1] M. Antonietti, C. Burger, M. A. Micha, M. Weissenberger, *Macromol. Chem. Phys.* **1999**, *200*, 150.
- [2] E. L. Thomas, B. A. Wood, *Faraday Discuss. Chem. Soc.* **1985**, *9*, 229.
- [3] T. Takahashi, F. Nagata, *J. Macromol. Sci., Phys.* **1989**, *B28*, 349.
- [4] M. Tokita, T. Takahashi, M. Hayashi, K. Inomata, J. Watanabe, *Macromolecules*, **1996**, *29*, 1345.
- [5] M. Tokita, K. Osada, M. Yamada, J. Watanabe, *Macromolecules* **1998**, *31*, 8590.
- [6] N. S. Murthy, S. M. Aharoni, *Macromolecules* **1992**, *25*, 1177.
- [7] H. Mensinger, A. Biswas, H. Poths, *Macromolecules* **1992**, *25*, 3156.
- [8] W. Ruland, *Colloid Polym. Sci.* **1977**, *255*, 417.
- [9] N. Stribeck, *Colloid Polym. Sci.* **1993**, *271*, 1007.
- [10] H. R. Kricheldorf, G. Schwarz, J. de Abajo, J. G. de la Campa, *Polymer* **1991**, *32*, 942.
- [11] H. Kricheldorf, R. N. Probst, C. Wutz, *Macromolecules* **1995**, *28*, 7990.
- [12] H. R. Kricheldorf, *Adv. Polym. Sci.* **1999**, *141*, 83.
- [13] C. Wutz, N. Stribeck, D. Gieseler, *Colloid. Polym. Sci.* **2000**, *278*, 1061.
- [14] S. Polizzi, N. Stribeck, H. G. Zachmann, R. Bordeianu, *Colloid. Polym. Sci.* **1989**, *267*, 281.
- [15] N. Stribeck, C. Wutz, *J. Polym. Sci., Part B: Polym. Phys.* **2001**, *39*, 1749.
- [16] H. R. Kricheldorf, N. Probst, G. Schwarz, C. Wutz, *Macromolecules* **1996**, *29*, 4234.
- [17] M. A. Micha, C. Burger, M. Antonietti, *Macromolecules* **1998**, *31*, 5930.
- [18] W. Ruland, *J. Appl. Cryst.* **1971**, *4*, 71.
- [19] N. Stribeck, S. Fakirov, D. Sapoundjieva, *Macromolecules* **1999**, *32*, 3368.
- [20] N. Stribeck, *J. Phys. IV* **1993**, *3*, 507.
- [21] N. Stribeck, H. G. Zachmann, R. K. Bayer, F. J. Baltà Calleja, *J. Mater. Sci.* **1997**, *32*, 1639.
- [22] J. J. Hermans, *Rec. Trav. Chim. Pays-Bas* **1994**, *63*, 211.
- [23] U. Dehlinger, A. Kochendörfer, *Z. Kristallograf.* **1939**, *101*, 134.
- [24] B. Crist, N. Morosoff, *J. Polym. Sci., Part B: Polym. Phys.* **1973**, *11*, 1023.
- [25] G. R. Strobl, N. Müller, *J. Polym. Sci., Part B: Polym. Phys.* **1973**, *11*, 1219.
- [26] N. Stribeck, W. Ruland, *J. Appl. Cryst.* **1978**, *11*, 535.
- [27] D. Gieseler, *Untersuchungen des Phasenverhaltens und der Kristallisation von Polyestern und Polyesterimiden mit Hilfe der Röntgenstreuung*, Ph.D. thesis, Universität Hamburg, 1999.